Two dimensional growth of ultrathin Fe films on BaTiO₃ with sharp chemical interface

G. Radaelli, M. Cantoni, Li Lijun, M. Espahbodi, and R. Bertacco

View Online   Export Citation   CrossMark

Two dimensional growth of ultrathin Fe films on BaTiO₃ with sharp chemical interface

G. Radaelli,[1] M. Cantoni,[1,a)] Li Lijun,[2] M. Espahbodi,[1] and R. Bertacco[1]

[1]*Dipartimento di Fisica, CNISM and LNESS, Politecnico di Milano, Via Anzani 42, 22100 Como, Italy*
[2]*Institute of Solid State Physics, Key Laboratory of Materials Physics, Chinese Academy of Sciences, Hefei 230031, People's Republic of China*

The Fe/BaTiO₃ interface is a prototypical artificial multiferroic system displaying purely electronic magnetoelectric effects at room temperature. As magneto-electric coupling is essentially localized at the interface, the properties of the very first Fe layers in contact with BaTiO₃ play a major role. In this paper, we investigate, by using X-ray photoemission spectroscopy and photoelectron diffraction, the *in-situ* growth, by molecular beam epitaxy, of ultrathin Fe films (∼7 monolayers) on a BaTiO₃/SrTiO₃(001) template. We found that growing the Fe films above room temperature (373 K) is essential in order to avoid island growth and obtain a continuous film. Post-annealing up to 473 K improves the film crystallinity but prevents chemical interdiffusion and roughening. Just an interfacial monolayer of oxidized iron is detected in these conditions, which appears as an unavoidable consequence of the Fe/BaTiO₃ chemical interaction. Its active role in magnetoelectric coupling must be carefully taken into account to correlate theoretical predictions and experiments. © 2014 AIP Publishing LLC. [http://dx.doi.org/10.1063/1.4864375]

I. INTRODUCTION

The search for room-temperature bulk multiferroic materials[1] and "artificial" multiferroic systems,[3] i.e., systems made of materials separately displaying different ferroic orders coupled to each other, currently generates strong theoretical and experimental efforts in condensed matter physics. This is crucial in view of the development of upcoming spintronic devices exploiting magnetoelectric coupling (MEC) to control the magnetic order acting on the ferroelectric one or *viceversa*.[4–6] For instance, multiferroics showing strong enough MEC could lead to spin-based devices with ultralow power consumption exploiting the electrical writing of the magnetic information, as well as novel microwave components. In the case of independent switching of the ferroic order parameters, multiferroics could also find applications as multiple-state data storage elements. However, a single-phase material showing a sizable coupling between ferromagnetism and ferroelectricity at room-temperature is still missing. A promising approach to circumvent the lingering scarcity of single-phase room-temperature multiferroics is combining ferroelectrics (FE) with ferromagnetic (FM) materials with high Curie temperatures to design interfacial multiferroics. In these systems, MEC is achieved at the interface between a FM and a FE.

Among many FM/FE heterostructures, Fe/BaTiO₃ has emerged as prototypical system. In fact, Fe and BaTiO₃ (BTO) possess robust ferroic orders at room temperature and a negligible lattice mismatch (∼1.6%), which favours epitaxial growth of Fe/BTO interfaces. Two kinds of ME coupling have been predicted at this interface: (i) direct coupling, owing to interfacial electronic effects, and (ii) indirect coupling, mediated by strain. The first one, leading to changes in the Fe surface magnetization and surface magnetocrystalline anisotropy, has been theoretically predicted and explained in terms of bond-reconfiguration driven by ionic displacement[7–9] or spin dependent screening mechanisms.[10] Experimentally it has been found that, for Fe thin films deposited on BTO single crystals, MEC is strain-mediated.[11,12] Large magnetic anisotropy and coercivity changes in the Fe layer have been reported in response to electric field applied to the BTO crystal because of its FE switching. However, fully epitaxial Fe overlayers on BTO films grown on other substrates are definitely more interesting in view of integration in practical devices. Recently, we have demonstrated[13] that, in these systems, mechanical clamping from the substrate suppresses the strain-mediated MEC, due to the suppression of BTO tetragons reorientation during FE transitions.[2,14] On the other hand, recent experimental reports suggest the existence of pure electronic interfacial MEC mechanisms in these fully epitaxial systems. Garcia *et al.*[15] demonstrated the nonvolatile electrical control of the tunnel magnetoresistance (TMR) in artificial Fe/BTO/La₂/₃Sr₁/₃MnO₃ (LSMO) multiferroic tunnel junctions (MFTJs) after switching the electrical polarization of the tunnel barrier, reflecting the modulation of the carriers spin polarization by the direction of FE polarization. In addition, evidence for remanent induced magnetic moments on Ti and O atoms, coupled with those of Fe, was observed in Fe/BTO/LSMO heterostructures by means of X-ray resonant magnetic scattering measurements.[8] More recently, we provided a direct experimental proof of the room temperature electrical "on-off" switching of the magnetic ordering within the interfacial oxidized Fe layer in contact with BTO in Co/Fe/BTO/LSMO heterostructures. By X-ray magnetic circular dichroism, we found that it is possible to create or suppress the ferromagnetic order just within the interfacial

a)Author to whom correspondence should be addressed. Electronic mail: matteo.cantoni@polimi.it

oxidized layer by reversing the dielectric polarization of the adjacent BTO.[16] In the same work, we found evidence for the tendency to island formation at the early stage of growth of ultrathin Fe films on BTO, which results also in a superparamagnetic behavior for low coverage (2 monolayers).

In this contest, the preparation and characterization of high-quality ultrathin Fe films on ferroelectric BTO layers are a fundamental achievement. In a pioneering work by Brivio *et al.*,[17] some of us reported on the epitaxial growth of 1–3 nm thick Fe films on $BaTiO_3/SrTiO_3(001)$. However, a complete study of the optimal growth conditions of Fe ultrathin films on BTO, with Fe thickness corresponding to few monolayers (MLs, where 1 ML corresponds to 0.143 nm, i.e., the lattice spacing between atomic planes in bcc Fe(001)), has not been reported so far. In particular, a study of the optimum conditions leading to 2D growth, good crystallinity and minimum interfacial oxidation of Fe is still missing.

In this paper, we investigate the growth mechanisms of ultrathin Fe films (about 1 nm thick) by Molecular Beam Epitaxy (MBE) on ferroelectric BTO films (50 nm thick) in terms of morphology, structural order, and oxidation. In particular, we optimized the growth conditions with respect to: (i) the substrate temperature (T_G) during Fe growth and (ii) the post-annealing temperature (T_{PA}) after Fe deposition. X-ray photoemission spectroscopy is employed to study the growth mode, layer-by-layer or by island nucleation, chemical interdiffusion and interfacial Fe oxidation, while X-ray photoelectron diffraction is used to investigate the structural order of the Fe film. We found that the room temperature growth gives rise to island formation, in agreement with our previous work,[16] while 2D growth is achieved just by growing films at $T_G = 373$ K. Post-growth annealing improves crystallinity up to $T_{PA} = 473$ K, while, at higher temperatures, sizable film corrugation is observed. Nevertheless, we do not find experimental evidence for chemical interdiffusion up to $T_{PA} = 673$ K. From the analysis of the Fe 2p lineshape, we detect the presence of just one monolayer (ML) of oxidized Fe at the interface with BTO, independently on the growth temperature (RT and 373 K) and post-annealing temperatures (up to 673 K). This indicates the high chemical stability of the interface, as well as the intrinsic chemical origin of the oxidized interfacial Fe ML, which results from the chemical bonds between Fe and BTO in these epitaxial structures.

II. EXPERIMENTAL

Fe/BTO heterostructures have been grown by Pulsed Laser Deposition (PLD) and MBE in a cluster tool, where the two deposition techniques are available *in-situ*, together with X-ray Photoemission Spectroscopy (XPS) and Diffraction (XPD) for investigating the chemical and structural properties of the samples, respectively.[18] BTO films, with thickness of 50 nm, have been grown onto $SrTiO_3$ (001) (STO) commercial substrates, according to a growth procedure optimized in order to obtain high quality ferroelectric epitaxial films with low surface roughness.[17,19] During the whole deposition process, the oxygen pressure has been kept at 2.67 Pa (0.02 Torr). Before the growth, an annealing of the substrate up to 1003 K has been performed for cleaning and ordering the surface, the temperature being controlled by a pyrometer. A quadrupled Q-Switched Nd:YAG laser (266 nm), providing pulses 7 ns long with a fluence of 5.6 J/cm^2, has been operated at a repetition frequency of 2 Hz to generate a plasma from a stoichiometric target placed in front of the substrate at a distance of 30 mm. The BTO growth, performed at 913 K, was followed by a post-annealing in 1 atm of oxygen at 873 K. The deposition rate in these conditions is 0.24 Å/pulse, as deduced from RHEED oscillations.

Fe overlayers with nominal thickness of 1 nm, corresponding to ∼7 ML, have been grown by MBE in ultra-high vacuum conditions (UHV), while keeping the substrate at room temperature (RT) or at 373 K. The Fe thickness has been calibrated by a quartz microbalance and checked by XPS after deposition. The Fe deposition rate was ∼0.15 nm/min. After deposition, the sample has been annealed for 20 min at different temperatures, up to 673 K.

The chemical and structural properties have been investigated *in-situ* by XPS and XPD. In XPS, photoelectrons were excited by standard unpolarized Al-K$_\alpha$ and Mg-K$_\alpha$ X-ray sources and collected by an Hemispherical Energy Analyzer (HEA) Phoibos 150 (SPECS^{TM}), yielding an acceptance angle of ∼6°, a field view of ∼1.4 mm^2, and an energy resolution of 1.03 eV and 0.84 eV for Al-K$_\alpha$ and Mg-K$_\alpha$, respectively. In XPD, the photoelectron were excited by Al-K$_\alpha$ and collected along the [100] azimuth, with an acceptance angle of ∼1°, a field of view of ∼1 mm^2 and an energy resolution of 1.5 eV. The Fe 2p core level has been chosen because the electron escape depth is 1.35 nm,[20] making it sensible to the whole Fe thickness for the films considered. The stability of the X-ray source during XPS and XPD measurements has been checked by measuring, at normal incidence, the XPS signal from a reference Ta sample. Film morphology has been investigated *ex-situ* by Atomic Force Microscopy (AFM).

III. RESULTS AND DISCUSSION

A. Fe growth mode and morphology

1. Fe 2p/Ti 2p

In order to check the Fe thickness and growth mode (layer-by-layer or by islands), the Fe 2p, Fe 3p, Ti 2p, Ba 3d, and O 1s features have been measured, as a function of the polar angle, by XPS with Al-K$_\alpha$ radiation. Here, we report the comparison between Fe and Ti intensities, but a similar trend is found when comparing Fe and O as well as Fe and Ba. In Fig. 1, are reported the ratios between the Fe 2p$_{3/2}$ and Ti 2p intensities, divided by the corresponding cross section and transmission of the analyzer, for sample #1 (panel (a)) and sample #2 (panel (b)), grown at RT and $T_G = 373$ K, respectively, as a function of polar collection angle for different values of T_{PA}. For comparison, the Fe 2p$_{3/2}$/Ti 2p (Fe/Ti from now on) theoretical ratio for a perfectly flat Fe film grown onto the BTO underlayer, represented by Eq. (1),[21] is also reported (blue line, dashed in panel (a) and continuous in panel (b)).
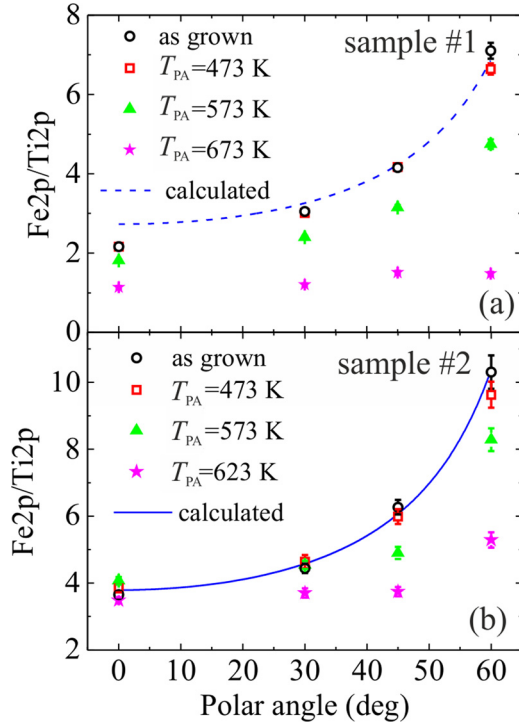
FIG. 1. Fe 2p/Ti 2p ratio for sample #1 (panel (a)) and sample #2 (panel (b)), grown at RT and 373 K, respectively, as a function of the post-annealing temperature (T_{PA}). The theoretical ratio for a perfectly flat Fe layer, according to Eq. (1), is also reported (blue line).

$$\frac{I_{Fe}}{I_{Ti}} = \frac{N_{Fe}}{N_{Ti}} \frac{\lambda_{Fe}}{\lambda_{Ti(BTO)}} \frac{1 - \exp(-d_{Fe}/\lambda_{Fe}\cos\theta)}{\exp(-d_{Fe}/\lambda_{Ti(Fe)}\cos\theta)}. \quad (1)$$

I_{Fe} and I_{Ti} are the Fe $2p_{3/2}$ and Ti 2p intensities, divided by the corresponding cross section and transmission of the analyzer; N_{Fe} and N_{Ti} are the Fe and Ti atomic densities; λ_{Fe} is the Fe $2p_{3/2}$ electron escape depth (13.5 Å (Ref. [20])); $\lambda_{Ti(BTO)}$ and $\lambda_{Ti(Fe)}$ are the Ti 2p electron escape depths in BTO (19.4 Å (Ref. [20])) and Fe (16.6 Å (Ref. [20])); d_{Fe} is the Fe thickness.

From the comparison of panels (a) and (b) of Fig. 1, a clear difference appears between samples #1 and #2 *as-grown*. Even though the nominal thickness is the same (1 nm ± 0.1%, which is the typical accuracy of our growth rates calibrated with a quartz microbalance), the Fe/Ti intensity ratio is 2.2 for sample #1 and 3.6 for sample #2. Furthermore, a good fit with Eq. (1), using the expected values for parameters listed above, is possible only for sample #2 (compare the blue continuous line in panel (b) with the dashed one in panel (a)). From the exponential fit, we can then estimate the Fe thickness only for sample #2 ($d_{Fe} = 1.04 \pm 0.04$ nm), in good agreement with our calibrated growth rate. These findings definitely signal a completely different growth mode in the two cases, with a clear deviation from the 2D mode for sample #1.

Looking now at the effect of post-annealing, for both samples #1 (panel (a)) and #2 (panel (b)), we observe that the films *as-grown* (black dots) and after post-annealing at $T_{PA} = 473$ K (red squares) are quite similar in terms of the Fe/Ti ratio: we can then conclude that this first annealing (up to 473 K) does not produce sizable chemical interdiffusion

nor morphology modifications of the Fe film. At larger annealing temperatures, instead, major modifications of the Fe/Ti ratio are seen. For sample #1 (Fig. 1(a)), the value at 0° strongly decreases (from 2.2 to 1.1) and also the slope of the Fe/Ti ratio vs. collection angle is progressively reduced, ending up with an almost flat behaviour at $T_{PA} = 673$ K. For sample #2 (Fig. 1(b)), the value at 0° is instead constant, within the error bar, while the slope of the curve vs. collection angle still decreases as T_{PA} increases, so that fitting with Eq. (1) gives in any case inaccurate results. From this analysis, it is clear that a 2D film with uniform thickness can be obtained only in case of sample heating during growth, while RT growth followed by the same post-annealing cannot restore a 2D condition. For this reason, in the following, we will concentrate on sample #2 ($T_G = 373$ K), with the aim to assess the quality of the 2D films obtained at $T_{PA} = 473$ K as well as to understand the origin of the deviation of the Fe/Ti ratio from the 2D behaviour at higher annealing temperature.

2. Film roughening induced by post-annealing

The deviation from the 2D model of Fe/Ti ratio vs. collection angle seen at high T_{PA} can arise from two effects: chemical interdiffusion or film roughening. To rule out the first one, we carefully measured the Fe 2p, Fe 3p, Ti 2p, Ba 3d and O 1s peaks for all the post-annealing temperatures investigated. As a matter of fact, we did not find any trace of chemical shift nor line shape modification. The case of Fe 2p is reported in Fig. 4(b) (see below for a more detailed discussion), but the same behaviour is seen for all the other peaks from the chemical elements involved. This is a strong evidence for the absence of chemical interdiffusion promoted by post-annealing and proves the chemical robustness of the Fe/BTO interface, which is an essential ingredient in view of exploitation of MEC coupling. On the other hand, film roughening can easily explain the trend seen in Fig. 1(b): if post-annealing promotes the aggregation of Fe clusters, this leaves a portion of the film almost uncapped or with a lower coverage with respect to the nominal one, while a higher coverage is expected within the clusters. By consequence, the Fe signal decreases faster than in case of a continuous film, when increasing the collection angle. On the contrary, the Ti signal suffers from a lower attenuation, with respect to the case of the continuous Fe film, if some portions of BTO are almost uncapped or covered by a thinner Fe film. As a result, the Fe/Ti ratio vs. collection angle is expected to be lower for a rough Fe film than for a continuous, uniform film. This is exactly what is seen in Fig. 1, both for sample #1 and sample #2, thus indicating an increase of roughening when increasing T_{PA}. This is not surprising for metals grown onto oxides. For example, the evolution of the cluster dimensions and shape with annealing has already been observed in Fe/MgO[22] and has been explained by the temperature dependence of surface diffusion and Ostwald ripening.

We found direct evidence for this post-annealing induced film roughening by directly checking the surface roughness by *ex-situ* AFM. While 1 nm thick Fe film grown at 373 K (sample #2) and post-annealed at 473 K shows a r.m.s. roughness (measured on a 1 μm^2 area) lower than

0.15 nm, this increases up to 0.46 nm after annealing at 623 K. In this case, as seen in Fig. 2, the sample appears as made of Fe clusters with average diameter of 100 nm and 1.5 nm height, which are definitely compatible with the trend of XPS intensity ratios reported above. A similar topography, with sizable roughness, is found in case of films grown at RT (data not shown). Even though the interpretation of the phase contrast in AFM scans from samples exposed to atmosphere is not straightforward, some additional information can be extracted from our *ex-situ* AFM data in order to shed light on the peculiar growth mode (Volmer-Weber vs. Stransky-Krastanov, taking place at different T_G) and roughening process induced by post-annealing. In case of a pure Volmer-Weber (island growth) regime for RT growth, we would still expect to see a clear phase contrast between BTO capped and uncapped zones. However, this is definitely not the case: the phase signal is almost uniform over the entire sample area in rough samples. This suggests that an initial layer-by-layer growth of just the first Fe ML in contact with BTO could take place, followed by formation of metallic Fe islands, which is typical of the Stransky-Krastanov mode. Also in case of roughening induced by post-annealing, the oxidized wetting layer seems unaffected, while the roughening process could involve only the metallic overlayer. Obviously, there is no chance to disentangle metallic islands from the regions corresponding to the oxidized Fe wetting layer in contact with BTO, because our samples are exposed to atmosphere in order to perform *ex-situ* AFM. We expect instead a quite similar phase contrast from the whole Fe layer, which will be completely oxidized after air exposure, in agreement with our data. To summarize, our AFM data suggest that rough films are made of a uniform layer covering the substrate and clusters nucleating over them in case of room temperature growth or post-annealing at temperatures higher than 473 K.

B. Fe crystal structure

In Fig. 3, the XPD polar scans along the [100] azimuth of sample #2 after post-annealing at 473 K (black), 573 K (red), and 623 K (green) are reported. For comparison, the scan from a bulk Fe(001) single crystal is also shown (blue line). At the kinetic energy of Fe 2p photoelectrons (778 eV), forward scattering dominates; thus the main diffraction peaks correspond to the crystallographic directions of the more dense atomic chains, as shown in the inset. Noteworthy, the XPD patterns are well defined, with sharp
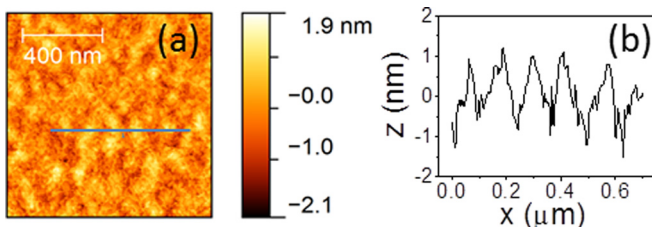
FIG. 2. (a) Atomic force microscopy image (1 μm^2 area) surface of a 1 nm thick Fe film grown at 373 K (sample #2) and post-annealed at 623 K (the vertical scale range is 4 nm); (b) surface profile corresponding to blue line in the atomic force microscopy image in (a).
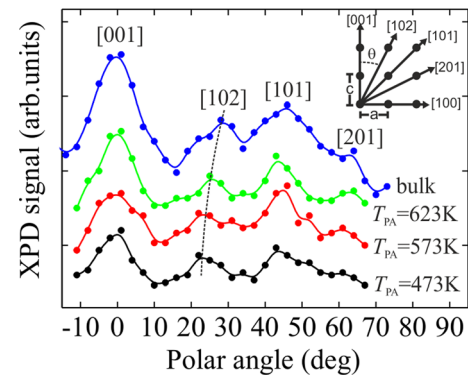
FIG. 3. XPD polar scans along the [100] azimuth of sample #2 as a function of the post-annealing temperature T_{PA}; for comparison, the scan from a bulk Fe(001) is also shown (blue line). The crystallographic directions corresponding to the main diffraction peaks, as shown in the inset, are reported.

peaks emerging from the background, for all the post-annealing conditions. Moreover, the film annealed at $T_{PA} = 623$ K (green line) looks better, in terms of peak sharpness, than that annealed at $T_{PA} = 473$ K (black line), despite the higher roughness of the former. This apparent contradiction can be explained considering that XPD is intrinsically a short-range probe of crystal structure, being sensible to the very local structure (the coherence length of XPD is few electron mean free paths) around the photo-electron emitters. Because the island dimension ($\sim$100 nm, according to AFM) is larger than few electron mean free paths ($\lambda_{Fe2p} = 1.35$ nm (Ref. 20)), their structure does not sensibly affect the XPD pattern. Post-annealing then promotes the film roughening but also improves the local crystal order. In fact, our XPD data indicate that strain relaxation takes place within the islands. Fe grows on BTO with 45° rotation, that is, the [100] direction of Fe is parallel to the [110] direction of BTO.[17] The bulk lattice parameter of Fe is $a_{Fe} = 2.87$ Å, while the in-plane lattice parameter of BTO is $a_{BTO} = 3.992$ Å, leading to a 1.6% lattice mismatch (considering the 45° rotation). In a single-scattering picture and considering only forward scattering events, the position of the main diffraction peaks can be found by geometrical considerations. As shown in the inset of Fig. 3, the angular positions of the [102], [101], and [201] peaks of Fe can be calculated as $\theta = \tan^{-1}(a/2c)$, $\tan^{-1}(a/c)$, and $\tan^{-1}(2a/c)$, where the a and c are in-plane and out-of-plane lattice parameters of Fe, respectively. In the bulk case, we have $a = c$ and the calculated angular positions are $\theta = 26.6°$, 45°, and 63.4°, respectively, coincident (within our experimental accuracy of $\pm 1°$) with the experimental ones (blue curve). If we assume that Fe grows compressed on BTO in order to fit with the BTO surface lattice, instead, we would have $a < c$, leading to peaks lying at smaller angles than in bulk Fe. As a matter of fact, looking at the experimental XPD scan in Fig. 3, we note that the peaks from Fe films on BTO are always found at smaller angles with respect to bulk Fe. Nevertheless, a clear shift towards the bulk position is seen when increasing T_{PA}. This is particularly evident for [102] peak that, being the closest to normal incidence, is less affected by border effects due to cluster's sides: when T_{PA} increases from 473 K to 623 K, it shifts from 21° to 24°. This

behaviour is consistent with a partial strain relaxation via dislocations within the Fe islands appearing at high post-annealing temperature. Thus, we can conclude that post-annealing above 473 K reduces the long-range order, inducing the formation of Fe clusters, but is accompanied by an improvement of the short-range order, leading to Fe clusters with a local structure closer to that of bulk Fe than continuous films. Note also that this is an additional indication of the absence of sizable interdiffusion induced by post-annealing, which would instead negatively affect XPD, due to the short-range nature of this technique.

C. Fe oxidation

In order to evaluate the Fe oxidation in Fe/BTO samples, in Fig. 4, we report the Fe 2p spectra, measured by XPS with Mg-K$_\alpha$ radiation, corresponding to the different T_G and T_{PA} discussed above. A Shirley background has been subtracted to all the curves and their intensities have been normalized to the peak value for each spectrum. In panel (a) we compare sample #1 (red curve) and sample #2 (black curve), grown at RT and $T_G = 373$ K, respectively, without any post-annealing treatment. The two spectra are essentially equivalent, without any noticeable dependence on T_G. In the inset, we compare the Fe 2p spectrum from sample #2 annealed at 473 K (black empty dots) with two reference spectra obtained from clean Fe(001) (blue curve) and
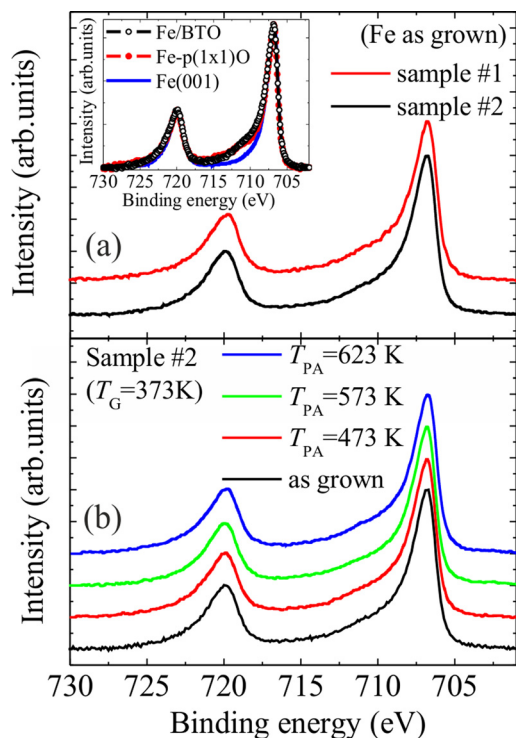

FIG. 4. Fe 2p spectrum measured by XPS: (a) samples #1 (red line) and #2 (black line) as-grown (at RT and $T_G = 373$ K, respectively); (b) sample #2 as-grown (black line) and post-annealed at different temperatures (red, green, and blue lines). In the inset of panel (a), we report the Fe 2p spectrum from sample #2 annealed at 473 K (black empty dots) and two reference spectra obtained from clean Fe(001) (blue curve) and Fe(001)-p(1×1)O surfaces (red full dots), respectively. A Shirley background has been subtracted to all the spectra and the vertical scale has been renormalized in order to have the same peak height for all the spectra.

Fe(001)-p(x1)O surfaces (red full dots),[23] respectively. The latter corresponds to just one ML of oxygen adsorbed onto a Fe(001) surface, and can be assumed as absolute reference for calibrating the thickness of the interfacial oxidized Fe layer at the interface with BTO.[24] It is clear, from comparison with Fe(001)-p(x1)O, that our Fe film is partially oxidized, due to the appearance of a shoulder at ~711 eV in addition to the metallic main peak at 707 eV. From the position of this shoulder, it is hard to identify the chemical state corresponding to these oxidized atoms. Any attribution of Fe valency based on the tabulated positions of Fe^{2+} or Fe^{3+} components in oxides would be inappropriate, because we are dealing with an ultrathin oxidized Fe layer strongly interacting with BTO, so that even the crystal field is definitely different from that of Fe oxides. As suggested in literature[25] and by XAS measurements by our group on ultrathin Fe/BTO films (see Refs. 16 and 26), we can affirm that this Fe oxidation is confined at the interface and involves about one Fe ML. This can be inferred from the strict similarity between our Fe spectrum (black empty dots) and that of Fe(001)-p(x1)O (red full dots). Despite the two geometries are different (in the case of Fe(001)-p(1x1)O, the oxygen ML is on top of bulk Fe, while for Fe/BTO it is below 1 nm of Fe) a straightforward calculation (see Appendix), based on the exponential attenuation of the photoelectron signal in a layer by layer model (which is suitable for the interpretation of spectra from sample #2 annealed up to 473 K) shows that the expected relative intensities of the oxidized and metallic components should be the same in the two cases, within $\pm 5\%$. This is exactly what we observe experimentally, thus providing an additional proof of the presence of just one oxidized Fe layer.

Finally, in panel (b), we compare sample #2 as-grown (black curve) and after post-annealing at different temperatures: $T_{PA} = 473$ K (red curve), 573 K (green curve), and 623 K (blue curve). Even in this case, the spectra are equivalent. We can then conclude that the Fe oxidation is independent on both T_G (RT or 373 K) and T_{PA} (up to 623 K). The fact that the relative intensities of the oxidized and metallic components are the same, whatever the film is flat or with clusters, is coherent with the layer + island growth mode and with a roughening process involving only the metallic Fe overlayer, as suggested by AFM data. According to these growth and roughening modes, the number of oxidized atoms does not change in the different conditions of growth and post-annealing, as it corresponds to the atoms of the first Fe ML in contact with BTO. On the other end, we expect very similar intensity ratios between the oxidized and metallic components in Fe 2p spectra, both in case of a single ML of oxidized Fe capped with a more uniform metallic Fe overlayer (e.g., sample #2 as-grown) or with some islands of metallic Fe. In rough films, islands strongly attenuate the signal from the oxidized layer underneath, while regions without islands do not present any attenuation of the signal from oxidized iron atoms. We can then expect a compensation between uncapped and capped regions in rough films (e.g., sample #1), thus leading to an average signal from the oxidized Fe layer which is very similar to that from flat, continuous Fe films (sample #2 up to 473 K).

To summarize, our data provide evidence for the presence of just one ML of oxidized Fe at the interface with BTO, which is extremely stable and independent on the sample growth recipe or post-annealing treatment. This is a strong indication of the intrinsic nature of this interfacial oxidation, appearing not a spurious artefact coming from non-optimized growth conditions but the unavoidable consequence of the chemical bonds between Fe and BTO upon the interface formation.

IV. CONCLUSIONS

In this paper, we investigated, by XPS and XPD, the MBE growth of ultrathin Fe films (about 1 nm) on a BaTiO$_3$/SrTiO$_3$(001) template, in order to evidence the influence on morphology, structural order, and oxidation of the growth and post-annealing temperatures. We found that the optimal conditions for obtaining 2D films are: (i) keeping the substrate at 373 K during Fe deposition; (ii) performing a post-annealing of the sample for 20 min at 473 K. Larger post-annealing temperatures lead instead to film roughening, but the local ordering, as checked by XPD, improves when the post-annealing temperature increases and clustering takes place. No trace of chemical interdiffusion is seen up to the highest post-annealing temperature investigated (673 K), while a minor Fe oxidation (just one ML confined at the interface) is present, not affected neither by the growth nor by the post-annealing temperatures. Our results clearly point to the high robustness and chemical stability of the Fe/BTO interface, intrinsically including one ML of oxidized Fe, which is an essential ingredient for its exploitation within devices based on interfacial magneto-electric coupling effects.

APPENDIX: CALCULATION OF THE INTENSITY RATIO BETWEEN OXIDIZED AND METALLIC IRON COMPONENTS

In this Appendix, we develop a simple model to calculate the expected relative intensities of the Fe oxidized and metallic components for two cases:

(1) Metallic Fe with thickness d_{Fe} on top of oxidized Fe with thickness d_{ox};
(2) Oxidized Fe with thickness d'_{ox} on top of semi-infinite metallic Fe.

We consider perfectly flat films and we make use a continuous model with exponential attenuation of the electron signal.

In case (i), the intensities of the metallic (Fe) and oxidized (Feox) components are

$$I_{Fe} = \alpha\lambda_{Fe}\left[1 - \exp\left(-\frac{d_{Fe}}{\lambda_{Fe}}\right)\right], \tag{A1}$$

$$I_{Feox} = \alpha\lambda_{Fe}\left[1 - \exp\left(-\frac{d_{ox}}{\lambda_{Fe}}\right)\right]\exp\left(-\frac{d_{Fe}}{\lambda_{Fe}}\right). \tag{A2}$$

λ_{Fe} is the electron escape depth of Fe 2p photoelectrons in Fe (we assume the same value for the metallic and oxidized components). α is a pre-factor depending on material parameters (cross section, density) and experimental conditions (photon flux, analyer transmission,…), and is equal for both the components. We are interested in the ratio I_{Feox}/I_{Fe}

$$\frac{I_{Feox}}{I_{Fe}} = \frac{\left[1 - \exp\left(-\frac{d_{ox}}{\lambda_{Fe}}\right)\right]\exp\left(-\frac{d_{Fe}}{\lambda_{Fe}}\right)}{1 - \exp\left(-\frac{d_{Fe}}{\lambda_{Fe}}\right)}. \tag{A3}$$

In case (ii), the intensities are

$$I_{Fe} = \alpha\lambda_{Fe}\exp\left(-\frac{d'_{ox}}{\lambda_{Fe}}\right), \tag{A4}$$

$$I_{Feox} = \alpha\lambda_{Fe}\left[1 - \exp\left(-\frac{d'_{ox}}{\lambda_{Fe}}\right)\right]. \tag{A5}$$

The ratio I_{Feox}/I_{Fe} is

$$\frac{I_{Feox}}{I_{Fe}} = \frac{1 - \exp\left(-\frac{d'_{ox}}{\lambda_{Fe}}\right)}{\exp\left(-\frac{d'_{ox}}{\lambda_{Fe}}\right)}. \tag{A6}$$

We now compare the I_{Feox}/I_{Fe} ratios for cases (i) and (ii). We employ $d_{ox} = d'_{ox} = 0.143$ nm (corresponding to 1 ML of oxidized Fe), $d_{Fe} = 0.9$ nm (the difference between the Fe thickness estimated in the Text for sample #2 annealed at 473 K, 1.04 nm, and the oxide thickness d_{ox}) and $\lambda_{Fe} = 1.35$ nm (see the main text and Ref. 20). Case (ii) corresponds to Fe-p(1×1)O (red full dots in the inset of Fig. 4).

From Eqs. (A3) and (A6), we obtain $I_{Feox}/I_{Fe} = 0.106$ for case (i) and $I_{Feox}/I_{Fe} = 0.112$ for case (ii), respectively. These results differ by 5% only: we can then conclude that, within the limit of our experimental accuracy, the relative intensities of the oxidized and metallic components are the same for the cases of 1 ML of oxidized Fe at the Fe/BTO interface (case (i), black empty dots in the inset of Fig. 4) and Fe-p(1×1)O (case (ii), red full dots in the inset of Fig. 4).

We note that, if we repeat the calculation with more than 1 ML of oxidized Fe at the interface in case (i), we would obtain a I_{Feox}/I_{Fe} ratio strongly different from that of case (ii), thus disagreeing with experimental results. If 2 ML of oxidized Fe are considered ($d_{ox} = 0.286$ nm and $d_{Fe} = 0.75$ nm, so that $d_{ox} + d_{Fe} \sim 1.04$ nm), we obtain $I_{Feox}/I_{Fe} = 0.255$ for case (i), more than two times the ratio

for case (ii). This analysis strongly supports our claim of the presence of just one ML of oxidized Fe at the Fe/BTO interface.

[1] S.-W. Cheong and M. Mostovoy, Nature Mater. **6**, 13–20 (2007); D. Khomskii, Physics **2**, 20 (2009); J. Magn. Magn. Mater. **306**, 1–8 (2006); M. Fiebig, J. Phys. D: Appl. Phys. **38**, R123–R152 (2005).

[2] H. Zheng, J. Wang, S. E. Lofland, Z. Ma, L. Mohaddes-Ardabili, T. Zhao, L. Salamanca-Riba, S. R. Shinde, S. B. Ogale, F. Bai, D. Viehland, Y. Jia, D. G. Schlom, M. Wuttig, A. Roytburd, and R. Ramesh, Science **303**, 661–663 (2004).

[3] F. Zavaliche, H. Zheng, L. Mohaddes-Ardabili, S. Y. Yang, Q. Zhan, P. Shafer, E. Reilly, R. Chopdekar, Y. Jia, P. Wright, D. G. Schlom, Y. Suzuki, and R. Ramesh, Nano Lett. **5**, 1793–1796 (2005).

[4] C. A. F. Vaz, J. Hoffman, C. H. Ahn, and R. Ramesh, Adv. Mat. **22**, 2900 (2010).

[5] M. Bibes, Nature Mater. **11**, 354–357 (2012).

[6] J. P. Velev, S. S. Jaswal, and E. Y. Tsymbal, Philos. Trans. R. Soc. A **369**, 3069–3097 (2011).

[7] C.-G. Duan, S. S. Jaswal, and E. Y. Tsymbal, Phys. Rev. Lett. **97**, 047201 (2006).

[8] C.-G. Duan, J. P. Velev, R. F. Sabirianov, W. N. Mei, S. S. Jaswal, and E. Y. Tsymbal, Appl. Phys. Lett. **92**, 122905 (2008).

[9] S. Valencia, A. Crassous, L. Bocher, V. Garcia, X. Moya, R. O. Cherifi, C. Deranlot, K. Bouzehouane, S. Fusil, A. Zobelli, A. Gloter, N. D. Mathur, A. Gaupp, R. Abrudan, F. Radu, A. Barthélémy, and M. Bibes, Nature Mater. **10**, 753 (2011).

[10] C.-G. Duan, J. P. Velev, R. F. Sabirianov, Z. Zhu, J. Chu, S. S. Jaswal, and E. Y. Tsymbal, Phys. Rev. Lett. **101**, 137201 (2008).

[11] S. Sahoo, S. Polisetty, C.-G. Duan, S. S. Jaswal, E. Y. Tsymbal, and C. Binek, Phys. Rev. B **76**, 092108 (2007).

[12] S. Brivio, D. Petti, R. Bertacco, and J. C. Cezar, Appl. Phys. Lett. **98**, 092505 (2011).

[13] G. Radaelli, D. Petti, M. Cantoni, C. Rinaldi, and R. Bertacco, "Absence of strain-mediated magnetoelectric coupling at fully epitaxial Fe/BaTiO₃ interfaces," J. Appl. Phys. (in press).

[14] D. G. Schlom, L. Q. Chen, C. B. Eom, K. M. Rabe, S. K. Streiffer, and J. M. Triscone, Annu. Rev. Mater. Res. **37**, 589 (2007).

[15] V. Garcia, M. Bibes, L. Bocher, S. Valencia, F. Kronast, A. Crassous, X. Moya, S. Enouz-Vedrenne, A. Gloter, D. Imhoff, C. Deranlot, N. D. Mathur, S. Fusil, K. Bouzehouane, and A. Barthélémy, Science **327**, 1106 (2010).

[16] G. Radaelli, D. Petti, E. Plekhanov, I. Fina, P. Torelli, B. R. Salles, M. Cantoni, C. Rinaldi, D. Gutiérrez, G. Panaccione, M. Varela, S. Picozzi, J. Fontcuberta, and R. Bertacco, "Electric control of ferromagnetic order at the Fe/BaTiO₃ interface," Nature Commun. (submitted).

[17] S. Brivio, C. Rinaldi, D. Petti, R. Bertacco, and F. Sanchez, Thin Solid Films **519**, 5804–5807 (2011).

[18] R. Bertacco, M. Cantoni, M. Riva, A. Tagliaferri, and F. Ciccacci, Appl. Surf. Sci. **252**, 1754 (2005).

[19] G. Radaelli, S. Brivio, I. Fina, and R. Bertacco, Appl. Phys. Lett. **100**, 102904 (2012).

[20] S. Tanuma, C. J. Powell, and D. R. Penn, Surf. Interface Anal. **17**, 911 (1991).

[21] C. S. Fadley, R. J. Baird, W. Siekhaus, T. Novakov, and S. A. L. Bergström, J. Electron Spectrosc. Relat. Phenom. **4**, 93 (1974).

[22] R. Reitinger, B. Sepiol, G. Vogl, B. Pfau, L.-M. Stadler, S. Stankov, F. Zontone, N. Spiridis, and J. Korecki, J. Appl. Phys. **102**, 034310 (2007).

[23] A. Cattoni, D. Petti, S. Brivio, M. Cantoni, R. Bertacco, and F. Ciccacci, Phys. Rev. B **80**, 104437 (2009).

[24] R. Bertacco and F. Ciccacci, Phys. Rev. B **59**, 4207 (1999).

[25] L. Bocher, A. Gloter, A. Crassous, V. Garcia, K. March, A. Zobelli, S. Valencia, S. Enouz-Vedrenne, X. Moya, N. D. Marthur, C. Deranlot, S. Fusil, K. Bouzehouane, M. Bibes, A. Barthélémy, C. Colliex, and O. Stéphan, Nano Lett. **12**, 376–382 (2012).

[26] C. Rinaldi, Il Nuovo Cimento C **4**, 71 (2013).